

Article

Deformation Modeling of Flexible Pavement in Expansive Subgrade in Texas

Asif Ahmed ^{1,*} , MD Sahadat Hossain ², Pratibha Pandey ², Anuja Sapkota ² and Boon Thian ³

¹ State University of New York Polytechnic Institute (SUNY Poly), 100 Seymour Rd, Utica, NY 13502, USA

² Department of Civil Engineering, University of Texas at Arlington, 416 Yates Street, Arlington, TX 76019, USA; hossain@uta.edu (M.S.H.); pratibha.pandey@uta.edu (P.P.); anuja.sapkota@mavs.uta.edu (A.S.)

³ Texas Department of Transportation, Dallas, TX 76019, USA; boon.thian@txdot.gov

* Correspondence: asif.civil.buet.12@gmail.com

Received: 26 August 2019; Accepted: 16 October 2019; Published: 18 October 2019



Abstract: The tendency of expansive subgrade soil to undergo swelling and shrinkage with the change in moisture has a significant impact on the performance of the pavement. The repeated cycles of wet and dry periods throughout a year lead to considerable stress concentration in the pavement subgrade soil. Such stress concentrations lead to the formation of severe pavement cracks. The objective of the research is to develop a prediction model to estimate the deformation of pavement over expansive subgrade. Two pavement sites—one farm to market road and one state highway—were monitored regularly using moisture and temperature sensors along with rain gauges. Additionally, geophysical testing was performed to obtain a continuous profile of the subgrade soil over time. Topographical surveying and horizontal inclinometer readings were taken to determine pavement deformation. The field monitoring data resulted in a maximum movement up to 80 mm in the farm to market road, and almost 38 mm in the state highway. The field data were statistically evaluated to develop a deformation prediction model. The validation of the model indicated that only a fraction of the deformation was reflected by seasonal variation, while inclusion of rainfall events in the equation significantly improved the model. Furthermore, the prediction model also incorporated the effects of change in temperature and resistivity values. The generated model could find its application in predicting pavement deformation with respect to rainfall at any time of the year.

Keywords: expansive subgrade; flexible pavement; deformation model; swelling; shrinkage; rainfall; Texas

1. Introduction

Construction of structures over expansive soil subgrade is common in several parts of the world [1]. Expansive subgrade tends to swell and shrink owing to the moisture variation resulting in the deformation of the structures built over it. There is a substantial annual cost of repair and maintenance of the structures built over expansive soil. About 9 billion to 15 billion USD is incurred as an annual cost associated with expansive soil. 50% of this cost comes from highways and streets [2–4]. Incorporation of expansive subgrade behavior into the design of pavements can significantly reduce the maintenance cost in future.

Almost 25% of the land in the United States is covered with expansive soil. Pavements in Texas, particularly North Texas, are plagued with expansive soil problems. One-fourth of the annual expenditure of Texas Department of Transportation (TxDOT) is spent in repair and maintenance of the problems associated with expansive soil. Expansive soil is usually unsaturated and clayey in nature [1]. It consists of three major minerals viz. kaolinite, illite, and montmorillonite. Montmorillonite clay are well known for high surface area, greater affinity to hold water, and

high plasticity [5]. These characteristics impart high swelling and shrinkage with moisture gain and dissipation, respectively, in such soil [6]. A significant amount of montmorillonite is reported in mid-zone of the USA [7]. Research by References [8] and [9] reported the presence of montmorillonite clayey soil in Dallas – Fort Worth area. This results in the volume expansion in wet season and shrinkage in dry season [6].

Volume change phenomenon in the expansive clayey subgrade leads to distresses in the pavement. The distresses are released in the form of cracking, heaving, and settlement of the pavement [1]. Longitudinal cracking, roughness, and fatigue cracking occur due to alternate cycles of volume expansion and contraction [10]. As moisture fluctuation is most susceptible in the pavement shoulder, it is most vulnerable to swelling and shrinkage resulting in pavement distresses [11,12]. Hence, longitudinal cracking in the pavement shoulder are the most prevalent pavement distress [10,13]. Provided the moisture change is uniform, the structure resting on expansive soil experience one-dimensional vertical movement. However, differential movement occurs because of varying moisture changes in different soil layers and different sections of the soil. Differential movement causes structural damage in buildings, highway pavements and airport pavements.

Deformation of expansive soil has been predicted either by laboratory studies or by numerical modeling by previous researchers [9,14]. Laboratory tests usually represent static conditions rather than actual field conditions. Numerical modeling of expansive soils requires special model type, i.e., cam-clay model for which critical state soil mechanics parameters are required such as modified compression and swelling index (λ , κ , etc.). However, limited studies have been carried out to develop a deformation model based on real-time deformation data. Real-time data accounts for all of the variability occurred at the field and incorporate dynamic changes due to climatic variations.

In this study, the deformation behavior of two different roads built on expansive subgrade in North Texas was investigated. The study was done on Farm to Market road (FM 2757) and State Highway (SH 342). Moisture sensors were installed at varying depths to capture the moisture variations. Additionally, Electrical Resistivity Imaging (ERI) was used to monitor seasonal moisture variations. Topographic survey and horizontal inclinometer survey were performed to observe the deformation behavior. This paper focuses on developing a pavement deformation model based on the behavior of expansive subgrade owing to the seasonal and temporal response. It portrays the monitoring results of two different roadways along with different parameters associated with deformation and develops a model through statistical analysis of the parameters.

In this paper, the main reason for volumetric change/deformation, which is moisture variation, is discussed in two test sites. Moisture variation through field instrumentation and resistivity imaging is presented in several sections. Furthermore, the effect of trees on the sides of the pavement is also discussed. The deformation behavior of two test sites is exhibited. In the next step, the deformation model was developed considering the effect of moisture, rainfall, seasonal variation, temperature, and suction. Additionally, the model was modified based on the response from field data. At last, the final model was validated using the field data.

2. Materials and Methods

2.1. Site Selection

The first site (FM 2757) was located in Kaufman county, Texas. The low volume, 2-lane road had no shoulder with small water bodies to both east and west side of the road. Surficial cracks were observed during preliminary investigation. Edge cracks of 3 inches wide and extending upto 12 inches depth in some locations were observed which indicated the presence of expansive subgrade soil.

Second site (SH 342) was situated in Lancaster, at the border between Dallas and Ellis county. Each lane was 11 ft wide with shoulder on each side. The pavement was flanked by grass and dense trees on both sides. No water bodies were observed nearby. Edge drops upto several inches were observed in the pavement shoulder.

2.2. Subsurface Exploration

Subsurface conditions at both sites were investigated collecting soil samples by boring. Three borings were done at each site, and general soil classification tests were conducted. Atterberg limit, moisture content test, and Scanning Electron Microscopy (SEM) were also carried out. Hitachi 3000 N SEM Microscope, equipped with energy dispersive X-ray (EDX) detector was used for detailed composition. For better understanding, both 500 × and 1000 × magnifications were adopted.

2.3. Deformation Monitoring

The deformation of the pavement was monitored through monthly topographic surveys and horizontal inclinometer survey. A topographical survey provides the overall surficial changes of the pavement profile while the inclinometer records the local deformation including the initiation of cracks and shoulder movement [11]. A topographical survey compares the surveys taken at regular intervals with the initial profile of the pavement and gives the overall deformation. On the other hand, horizontal inclinometers provide the high-resolution movement of the pavement in the form of settlement or heave. The inclinometer can give full movement profile and precise measurements [15].

A Horizontal Digitilt inclinometer, manufactured by the Slope Indicator was used in this study. It consists of a horizontal probe, control cable, and a data mate. The reading was taken by passing the horizontal probe into 85 mm inclinometer casing installed in the trench across the pavement. The probe—consisting of two sensors 600 mm apart—measures the tilting angle of the device from the horizontal baseline. The movement of the pavement was thus determined with the change in inclination. The accuracy of the measurement was within the range of $\pm 0.01\%$ using the sinus law of the measured angle.

2.4. Moisture Monitoring by Field Instrumentation

The moisture variation in subgrade soil takes place due to various reasons of which the climatic loading such as precipitation, snowfall, etc. are the primary reasons. Among these climatic loading, snowfall is not a common phenomenon in the southern part of the USA including Texas. As such, precipitation can be considered as a major factor for moisture fluctuation in pavement subgrade for these regions. It is a reasonably accepted notion among the engineers that pavement performance is severely affected by environmental loading. However, quantitative analysis is limited [16]. For this, it is necessary to understand the moisture variation in subgrade with time. In this current study, moisture variation in the expansive subgrade that resulted in swelling and shrinkage phenomenon was captured installing dielectric moisture sensors. The dielectric moisture sensors used in this study provided the volumetric moisture content. Using the wet-volume relationship, the volumetric moisture content was converted to gravimetric moisture content. Throughout the manuscript, gravimetric moisture content is reported and discussed.

2.5. Seasonal Moisture Variation by Resistivity

Moisture sensors can only capture discrete moisture contents at the depth where they are installed. ERI, as geophysical testing was used to continuously profile the moisture variation beneath the pavement. It also allows the determination of moisture variation beneath the slope beside the pavements [12]. ERI measures the electric potential drop between two locations. Controlled current can be injected at a specific location and resistivity value can be calculated for the subsurface by measuring the drop in electric potential at other locations. However, the effect of non-homogenous soil mass and least path of resistivity for current flow should be duly considered.

Super-sting R8/IP resistivity meter from Advanced Geosciences Institute (AGI) and switch box with 12 volts battery for power supply were used for resistivity imaging. The resistivity imaging was carried out on a 24.7 m test line where the 28 electrodes were used at a spacing of 0.9 m. The dipole-dipole array was utilized which has been found to provide enhanced resolution in both vertical and horizontal

directions [17]. A forward modeling technique was applied in the Earth Imager 2D software [18] to compute the apparent resistivity values from the field data. The two-dimensional image of the subsurface is developed as a final output with the non-linear least squares optimization technique [12].

3. Results

3.1. Subsurface Results

Based on the Geologic Atlas Map of Texas, North Texas consists of sedimentary rock with smectite clay minerals and sulfates [6]. Researchers reported overburden residual soils linked with this formation usually consist of clay having high plasticity indices [19–21].

Collected soil samples were analyzed through sieves. It was observed in all samples that the clay content was above 85%, which indicates very fine subgrade soil. Atterberg limit tests yielded liquid limit between 50 and 64, whereas plasticity was ranged between 28 and 42. According to the Unified Soil Classification System (USCS), the soil was classified as high plastic clay (CH).

Based on the SEM analysis, the soil sample exhibited typical expansive soil structure (Figure 1a,b). The resulting spectra (Figure 1c) exhibited ample amount of Silicon (data not presented) which is in well agreement with the expansive soil microstructure study of Reference [22]. In addition, the expansive soil morphology (Figure 1a,b) was also compared with previous studies and similarity was obtained with papers such as Reference [23].

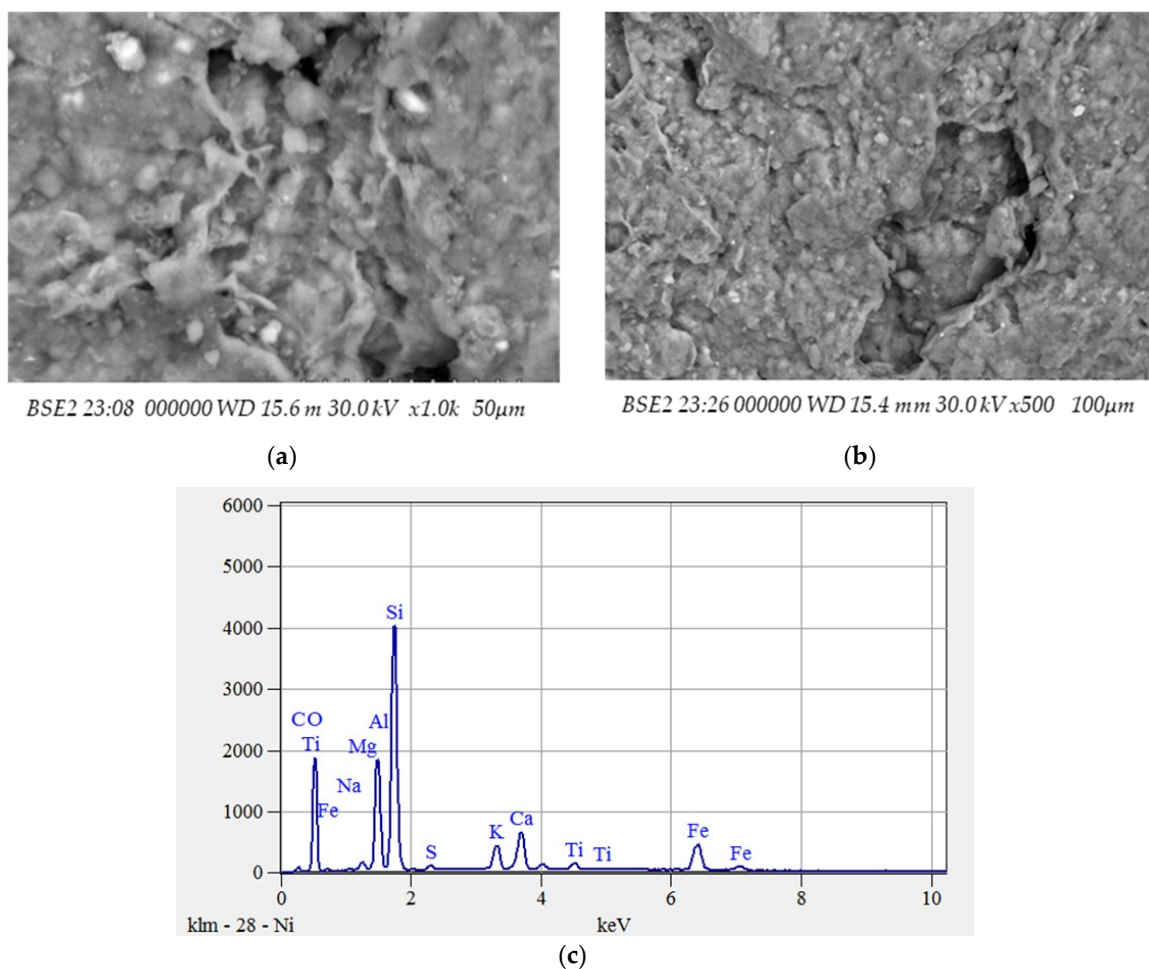
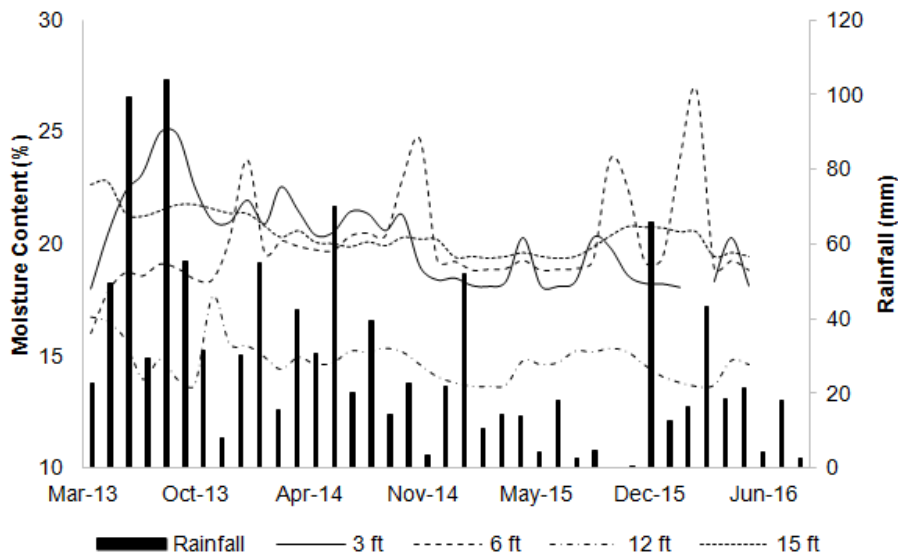


Figure 1. SEM micrographs of site soil at (a) 500 × magnification, (b) 1000 × magnification, and (c) EDX spectra of expansive soil (from several determinations).

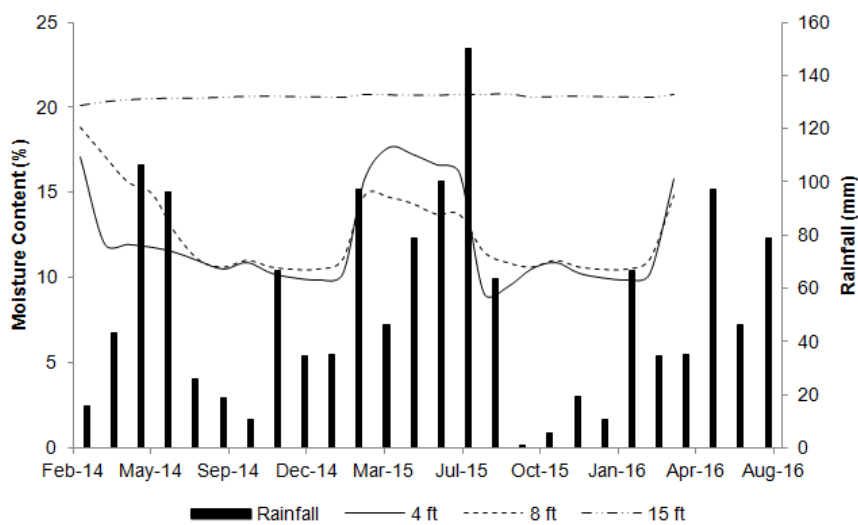
3.2. Moisture Variation in Center Borehole of FM 2757

Moisture content is a major variable for volumetric change in the expansive subgrade. It affects the change of material properties, i.e., resilient modulus of the soil. Hence, it is important to observe moisture variation of the subgrade with time. The moisture variations in center and edge borehole from FM 2757 and SH 342 roadway are described in the following sections.

Figure 2a depicts the variation of maximum moisture content in the borehole observed in the monitoring cycles. Highest moisture content was recorded at a depth of 6 ft and the lowest moisture content was recorded at a depth of 15 ft throughout the first phase. A similar pattern of moisture variation was observed for the remaining monitoring cycles. A minimal increase in maximum moisture variation curves was witnessed with the total rainfall as high as 4 inches from April to August 2013. The drop in maximum moisture curves was observed with decrease in rainfall. In general, the field monitoring results showed similar response to the rainfall events, the pattern of the maximum moisture variation curves and average moisture content values.



(a)



(b)

Figure 2. Moisture variation in (a) FM 2757 site and (b) SH 342 site.

3.3. Moisture Variation in Edge Borehole of SH 342

Figure 2b depicts the monthly change in average moisture content with the monthly cumulative rainfall for the sensors installed at different depth from 4 feet to 15 feet in the edge borehole. The change in moisture values with rainfall was observed for shallow sensors however, the deepest sensor exhibited constant moisture value of 21% throughout the monitoring period. The moisture variation at this level is restricted because of fully saturated condition. The observed minimal variation of moisture values for deep seated sensors is comparable to the observations made by References [24] and [13]. The sensors installed at 4 ft and 8 ft showed decline in moisture values in spite of the increase in precipitation by 3.6 inches. The sensor closer to the surface displayed 5% drop in average moisture values just from March to April while the deeper sensor exhibited gradual decrease. In August 2014, both the sensors data coincided with the 11% average moisture values. Moreover, the months from March to May in 2015 experienced increased rainfall events which resulted in increase moisture values up to 18% and 15% at 4 ft and 8 ft respectively. During summer 2015, the moisture values were dropped to 11% as recorded previously. The pattern was repeated again due to rainfall in March 2016 with the spike in moisture content.

3.4. Moisture Variation in Subgrade by Resistivity

The continuous image of the subgrade soil can be obtained with the Resistivity Imaging (RI) survey. The setup of the equipment is shown in Figure 3. It can produce moisture distribution at different levels and locations. Figure 4 shows the output from the resistivity imaging which can be interpreted with the resistivity values and its inverse relation to the moisture. The resistivity in the soil at different locations is indicated by the range of color from red to blue as seen in the figure. Higher resistivity corresponds to the low saturation while the lower resistivity represents the higher saturation in the soil. Figure 4a depicts the output from resistivity imaging performed during the months of May to October characterized by a high resistivity reading. This corresponds to the dry season of the year indicating more regions with less moisture. In contrast, the resistivity imaging performed during November to April which are the wet months gave image with low resistivity values as seen in Figure 4b. Moreover, RI was able to capture the area with cracks when performed immediately after the rainfall. In May 2016, the RI showed a region of low resistivity as seen in Figure 4c which was high resistivity region previously. This indicated the weakest region of subgrade soil from where the moisture intrusion takes place into the pavement system and needs maintenance.



Figure 3. Resistivity set up at slope of SH 342.

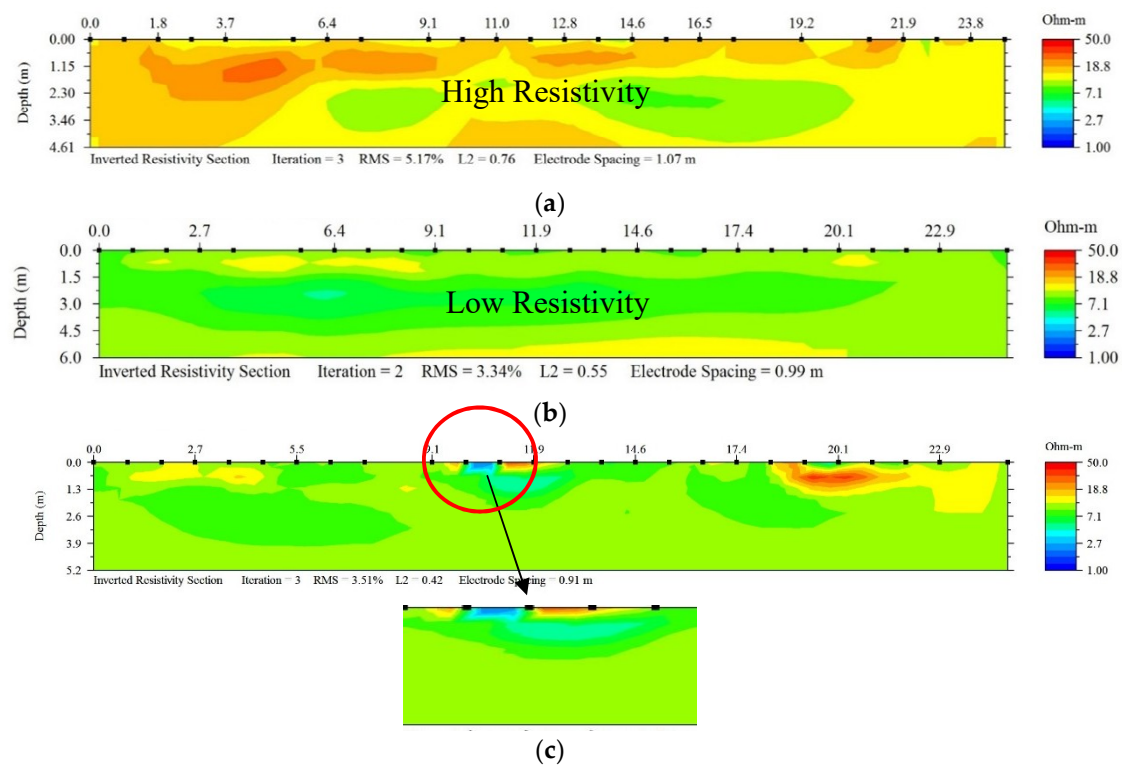


Figure 4. Resistivity variation in typical (a) dry period, (b) wet period, and (c) moisture intrusion through edge after rainfall.

The central section (at 12.8 m of Figure 4) of the resistivity profile was evaluated for one full cycle. Low resistivity of 7 to 13 Ohm m was observed between the months of November and April giving the high moisture values. This identified the period as the wet season. Reference [24] also identified the same period from November to April as wet period comparing the rainfall and evapotranspiration data. In the other hand, the dry season from May to October gave the resistivity value as high as 23 Ohm m. The moisture variation was found to follow the seasonal trend, which the moisture sensors were unable to capture. The resistivity does not seem to change significantly below 3 m identifying the depth as an active zone. This corroborates with the other studies performed in the same area which identified the depth from 3–3.66 m as an active depth [19]. Hence, the deformation is likely to take place in the active zone where the moisture and resistivity values changes during repeated drying and wetting period.

3.5. Moisture Intrusion from Edge of the Pavement

The contour of the moisture distribution has also been plotted to have a better insight upon the moisture flow in the subgrade soil (Figure 5). With the average moisture values, the peak values were suppressed and hence were not visualized in the plot shown in Figure 5a. However, the maximum moisture contour depicts the moisture intrusion from the edge of the pavement represented by blue zone (Figure 5b). This moisture infiltration from the edge leads to significant edge drop in the pavement. Therefore, the period of rainfall after the long summer days is considered a critical time for pavement deformation. The already opened shrinkage cracks in summer provide the pathway for the rainwater to intrude into the system.

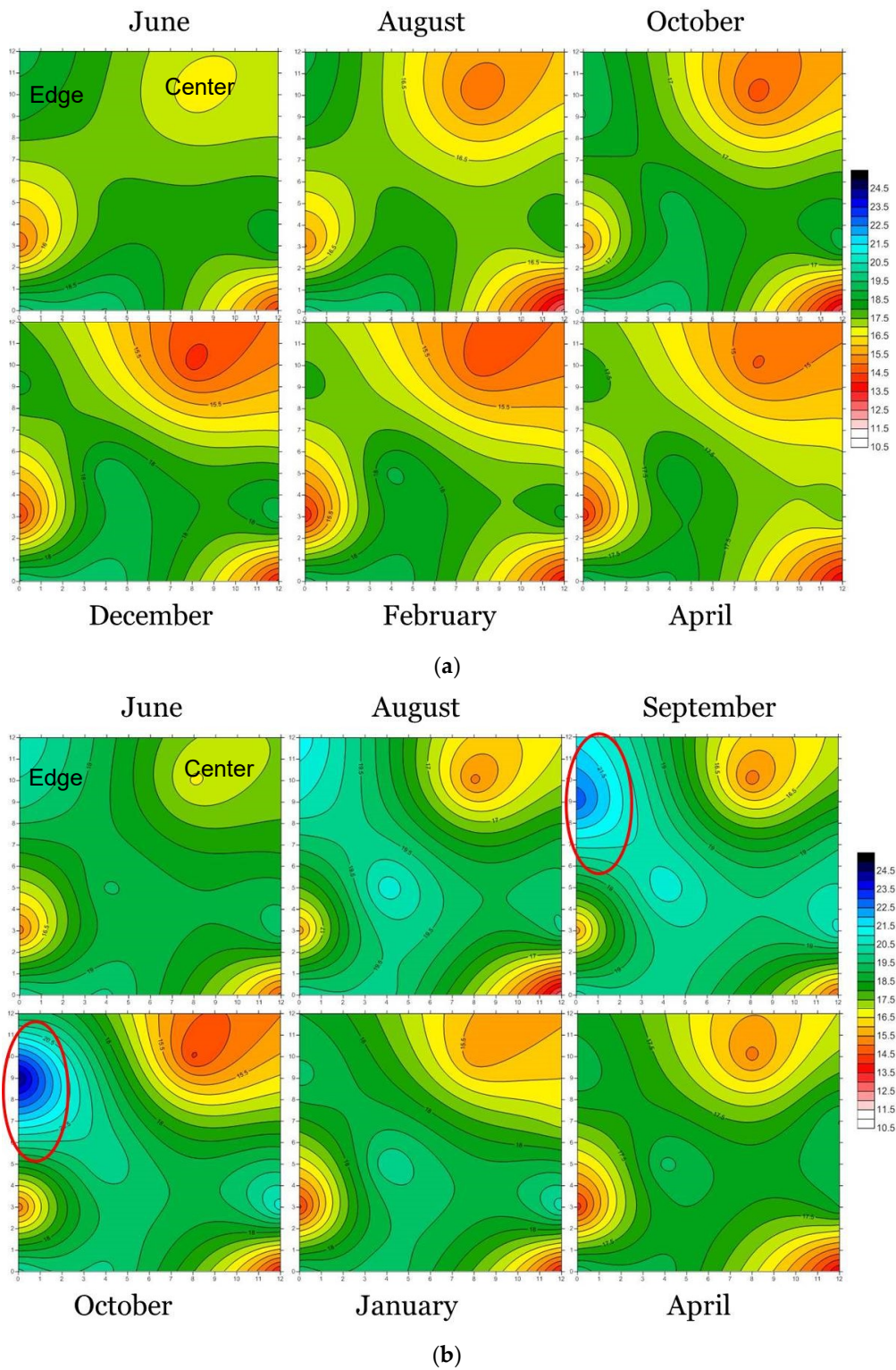


Figure 5. Bi-monthly (a) average moisture content and (b) maximum moisture content contour in pavement section.

3.6. Influence of Trees

The trees have been found to have impact on the shrinkage cracking of the flexible pavement from previous studies. Moreover, the trees are recommended to be planted at a safe distance from the infrastructures to avoid the probable damage with the shrinkage cracks [25]. In the UK, significant

shrinkage settlement was observed during severe drought due to moisture depletion caused by the surrounding trees. According to Reference [25], the trees near the pavement take up the moisture from the subgrade and causes moisture depletion ultimately leading to shrinkage cracks. The author proposed a “proximity rule” based on which the ratio of distance of tree from the edge of the structure to the height of tree i.e., D:H when reaches close to one, the trees would induce shrinkage cracks.

In the current study, both of the selected sites were surrounded by dense trees. Nonetheless, only the result from SH 342 has been presented here as both the sites showed similar findings (Figure 6). The figure compares the greenery at different times of year, i.e., summer and winter.



Figure 6. Comparison of roadside trees at SH 342 site in (a) summer and (b) winter.

The trees’ roots on the side of the pavement can move underneath the pavement for water. This was witnessed in two of the boreholes with a decrease in maximum moisture content as shown in Figure 7. Therefore, the trees can be considered as one of the factors contributing to pavement cracking at both sites.

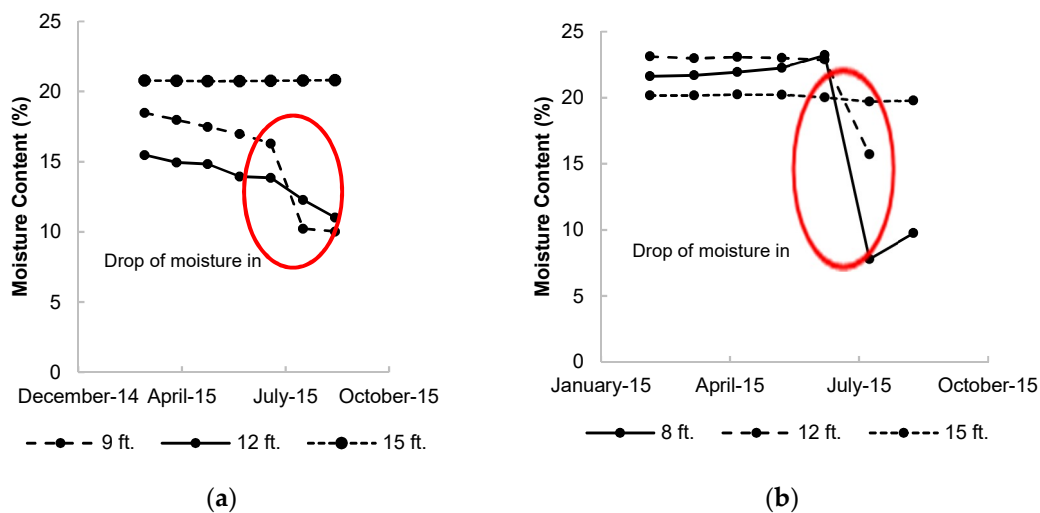


Figure 7. Drop of moisture content after summer at two boreholes of SH 342.

The D/H ratio of the trees in the State Highway was determined to be 0.91, with the height of trees approximately 34 ft and the distance of trees from the pavement cracks equal to 31 ft. Since the D/H ratio was close to 1, the site was experiencing the moisture depletion due to the presence of trees. With this, the summer period can be considered more critical when trees and grasses have more need for water and thus take up water from the soil resulting in desiccation of the expansive subgrade. This has also been observed in the result of resistivity imaging from May to July 2016. During this period, the resistivity has been found to increase, suggesting decrease in moisture content (Figure 4a,b).

However, the effect of trees has not been included in the deformation modeling as the study was limited to qualitative effect of trees.

Reference [26] performed a similar study on four pavement sites with highly plastic expansive subgrade soil. The pavement section in Paris with trees of an average height of 42 ft on the side was considered for analyzing the effect of large trees on pavement cracking. The trees were at a distance of 38 ft from the existing cracks in the pavement, giving the D/H ratio of 0.9, which is considered critical as stated by Reference [25]. This corresponded to the deteriorated condition of the pavements with large, long and deep cracks.

3.7. Deformation Behavior of FM 2757 Site

The monitoring of the pavement profile and its deformation was carried out using a horizontal inclinometer and topographical survey on a monthly basis. The first reading, taken in May 2012 was set as a zero-reference based on which the subsequent readings were assessed, and the movement of the pavement was evaluated.

The continuous monitoring of the pavement in FM 2757 indicated severe local deformations, along the edge of the pavement with the huge deformation recorded on a survey of September 22, 2013. The edge drop of 2 inches was observed during that time. This edge drop was followed by a huge crack. Similarly, the following summer of 2014 experienced edge drop in September. Moreover, the edge cracks were seen again in October 2015. The longitudinal cracks observed in the summer of 2014 and 2015 are shown in Figure 8. The crack depth was observed to be as deep as 7 inches.

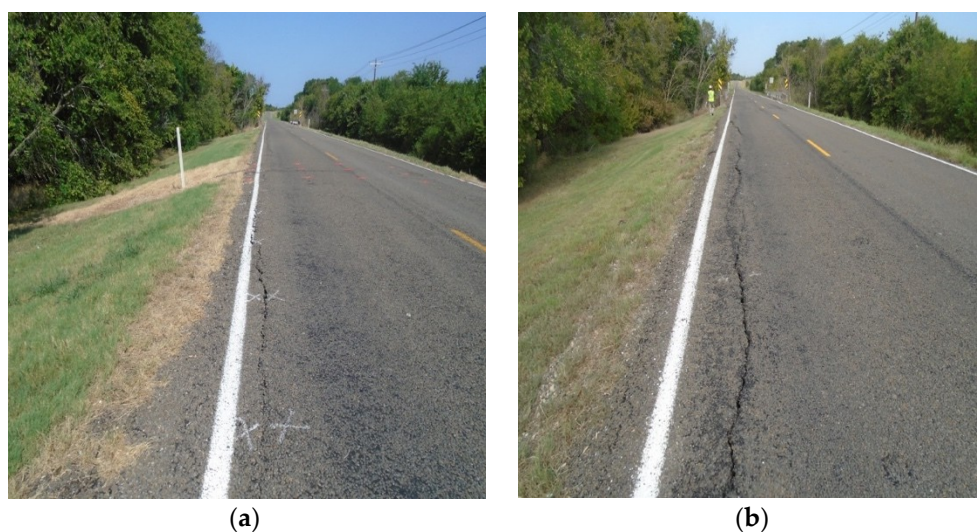


Figure 8. Crack after (a) Summer 2014 and (b) Summer 2015 at FM 2757 site.

3.8. Deformation Behavior of SH 342 Site

The deformation of the pavement in State Highway 342 was obtained using inclinometer which is shown in Figure 9. The upward and downward movement in the plot corresponds to the swelling and shrinkage of the expansive subgrade soil. The continuous monitoring of the site revealed 38 mm of vertical movement across the pavement as can be seen in Figure 9. However, there is no significant edge drop observed at this site due to support from the shoulder. The shoulder hindered the initiation of crack at the edge and prevented the excessive deformation of the pavement. The swelling and shrinkage were in the range of ± 50 mm. Similar seasonal trend was observed in both the sites i.e., FM 2757 and SH 342. The difference was only the presence of shoulder in the state highway, which was likely to prevent the excessive deformation in the pavement.

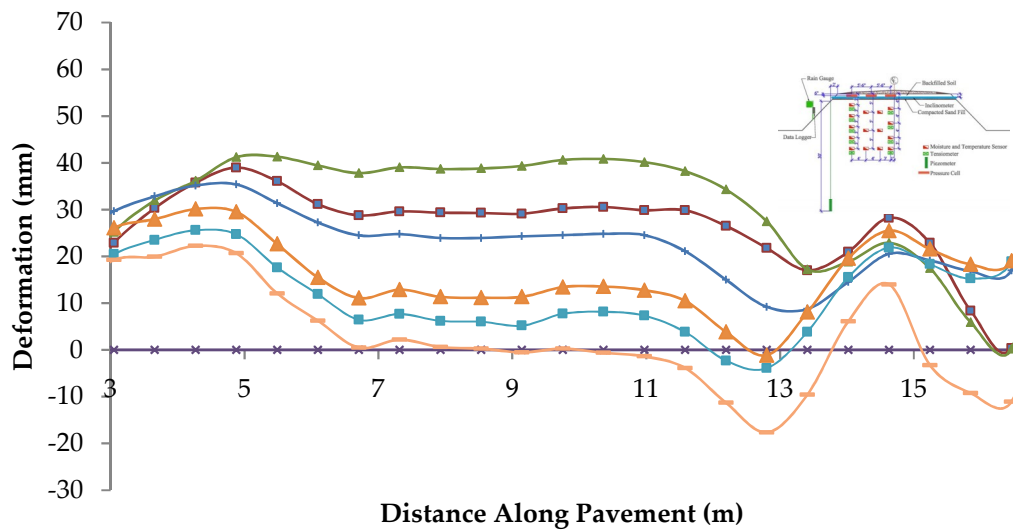


Figure 9. Variation of deformation along distance in central section in SH 342 site (from Inclinometer data).

3.9. Deformation with Rainfall at Both Sites

Figure 10a shows the pavement elevation at two points along the cross-section i.e., at the center and the cracked edge in FM 2757. The elevation of the pavement exhibited sensitivity to rainfall events, as can be seen in the figure. The swelling and shrinkage of the expansive subgrade soil were seen during the monitoring from 2014 to 2016. The swelling up to 60 mm was observed with the huge rainfall events from March to May 2015. The same amount of drop was observed immediately when no rainfall occurred from June to August 2015. The pavement deformation is dependent on both seasonal variation and precipitation as stated in previous studies [11,27].

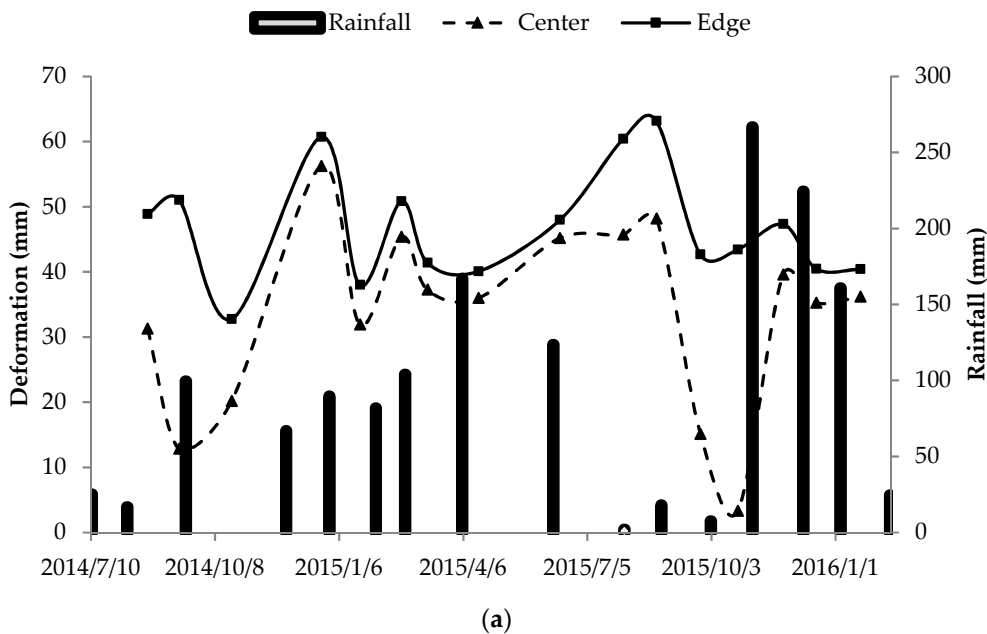


Figure 10. Cont.

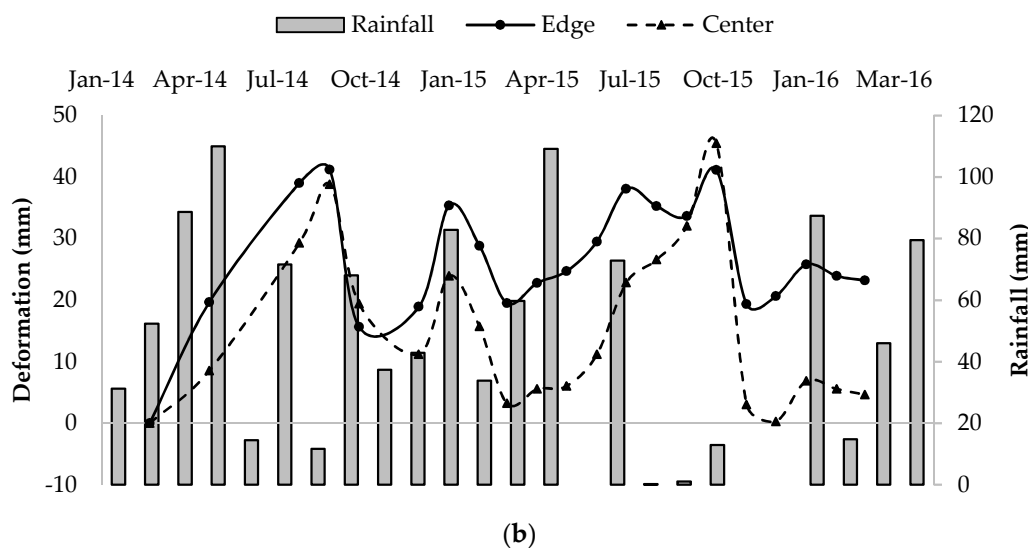


Figure 10. Deformation variation of edge and center with rainfall events at (a) FM 2757 and (b) SH 342 site.

The movement of the subgrade soil with the rainfall is shown in Figure 10b at two locations, i.e., left edge and center of SH 342. In general, the pattern of movement of subgrade soil at both the points corresponded to the rainfall event indicating the swelling and shrinkage behavior. For example, the cumulative rainfall of 114.3 mm from March to May 2014 resulted in swelling of 38.1 mm, while a drop of nearly one inch was witnessed after the summer of the corresponding year. A similar trend of swelling was captured in January 2015—with rainfall of almost 50 mm—which experienced a drop after October 2015 as a result of less rainfall at the site.

The continuous and repeated wetting and drying cycle exacerbates the condition of the pavement with upward and downward movement. Moisture balance is considered a prime criterion for such movement [11]. The evaluation of cracking potential based on the movement of these pavements can be useful in the design process as it describes the most vulnerable period for the pavement deterioration. Therefore, an attempt has been made to determine the cracking potential for the selected site.

Figure 11 shows the plot between the difference of elevation between the left edge and centerline of SH 342 pavement with time and rainfall. Here, the monitoring results from 2014–16 are only presented for evaluating the cracking potential. The plot shows the highest drop corresponding to the period with less rainfall (12.5 mm) in August 2014 and September 2014 leading to edge drop. A similar drop was witnessed again after September 2015. This proves that the rainfall amount has great impact on the cracking potential and the pavement has highest cracking potential in August and September based on the observation of the two pavement sites. Reference [28] also stated that crack opening usually occurs in the months from August to October in Central Europe.

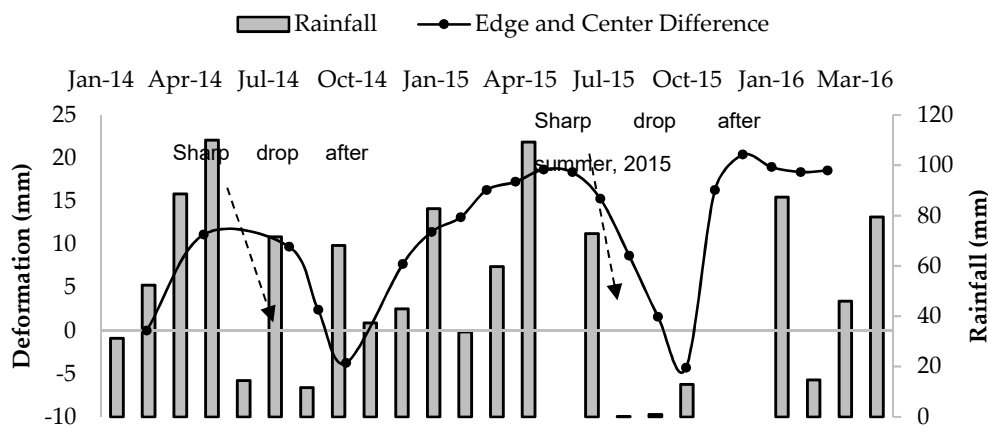


Figure 11. Edge drop at consecutive summer seasons at SH 342 site.

4. Development of Deformation Model

The instigation of shrinkage cracking in the pavement subgrade leads to cracks near the edge of pavement or its shoulder [29]. The authors [29] also stated that these types of longitudinal edge cracking are the most frequent type of pavement distress. Keeping this in view, although the whole pavement undergoes movement, only the edge was considered during model development. Additionally, the cracks initiate from the edge, which validates the consideration of only the edge for modeling.

4.1. Development of Initial Model

The first step was to define the predictor variables for developing the pavement deformation model, for which the effects of rainfall, moisture, suction, temperature and season of the year were considered. It is to be noted that the predictor variables should not correlate with each other [30]. Since rainfall is the main governing factor of moisture variation, both those variables could not be used for developing the model. Thus, only the effect of rainfall was considered for model development.

Temperature was then evaluated as a fit variable for using to predict deformation. Figure 12a depicts the change of temperature over several years for a single borehole. As can be seen, temperature was following more a seasonal trend than responding to rainfall. Pairs of temperature and corresponding deformation were assessed using both Pearson and Spearman correlation coefficient. The evaluation produced a Pearson coefficient of 0.438 and Spearman coefficient of 0.42. The p-value was found to be 0.047, which is less than 0.1 for a 10% confidence interval. This confirmed that the null hypothesis could be rejected that no significant relationship existed between the variables. For instance, Figure 12b, which presents the scatter plot between the variables, shows five different temperatures recorded for 20 mm deformation.

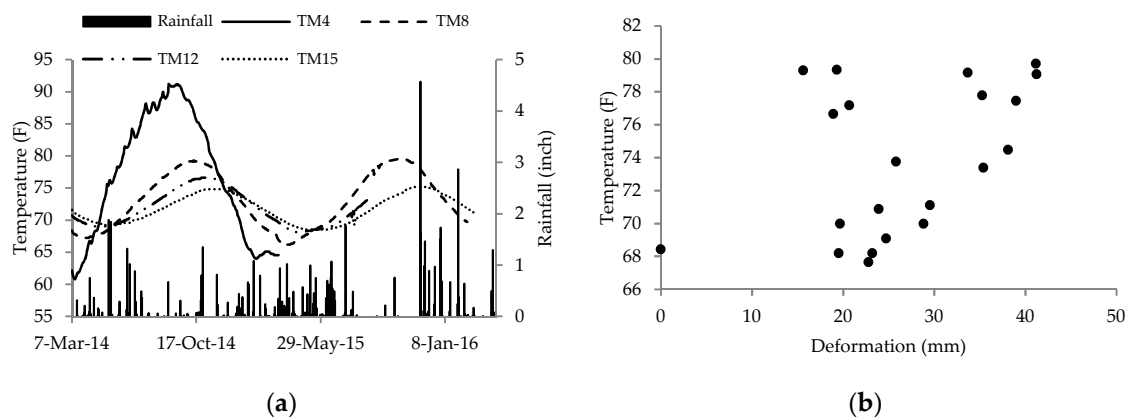


Figure 12. (a) Temperature variation in SH 342 site, and (b) Temperature and deformation plot for model development.

Suction values were then evaluated as a possible predictor variable and correlation with deformation was analyzed. There has always been a discussion regarding the reliability and longevity of suction sensors. Reference [26] stated that most of the water potential sensors measure the soil suction following the principle of thermal conductivity. This method relies on the potential energy of water in equilibrium with water in the soil [31]. A thermal conductivity sensor comprises of a porous ceramic block with temperature sensor and a heater. The water content of the block, which depends on the matric suction applied to the block by the surrounding soil, affects the thermal conductivity [32]. Since the two materials are then in equilibrium, the matric suction of the block will be same as of the surrounding soil. Previous research [26] shows the use of Fredlund Thermal Conductivity (FTC) sensor to measure field suction beneath a pavement slope. The author reported high failure rate of the sensors along with fragile ceramic used in the sensors. Another company manufactured water potential sensors to measure the matric suction of soil using the same principle but utilizing dielectric permittivity of solid matrix-porous ceramic disk. Air, solid ceramic and water have dielectric permittivity of 1, 5 and 80, respectively. The dielectric permittivity of the disk varies with the quantity of water present in the pore spaces of the disk. The ceramic used in MPS-1 sensor has a wide range of pore distribution. Thus, a substantial scale of moisture content can be covered by measuring the dielectric permittivity of the disk [31]. Nonetheless, the sensor can only record suction up to 10 kPa, which greatly limits the real-time actual field suction condition. References [33] and [34] stated that long-term suction monitoring is difficult and not reliable at times. References [33] and [34] thus predicted the ground movement based on water content. Additionally, the authors of Reference [27] reported field suction data for only ten months from March 2007 to June 2008, as other values were not available since the sensors had malfunctioned. Keeping in view all the above-mentioned findings, suction values were not considered as a predictor variable for model development. The authors of this manuscript also used suction sensors in field. As can be seen from Figure 13, most of the recorded values were clustered around 10 kPa for most of the time. Only sensors recorded at 3 ft depth exhibited some variation over time. The suction sensors was not responsive to rainfall like moisture sensors.

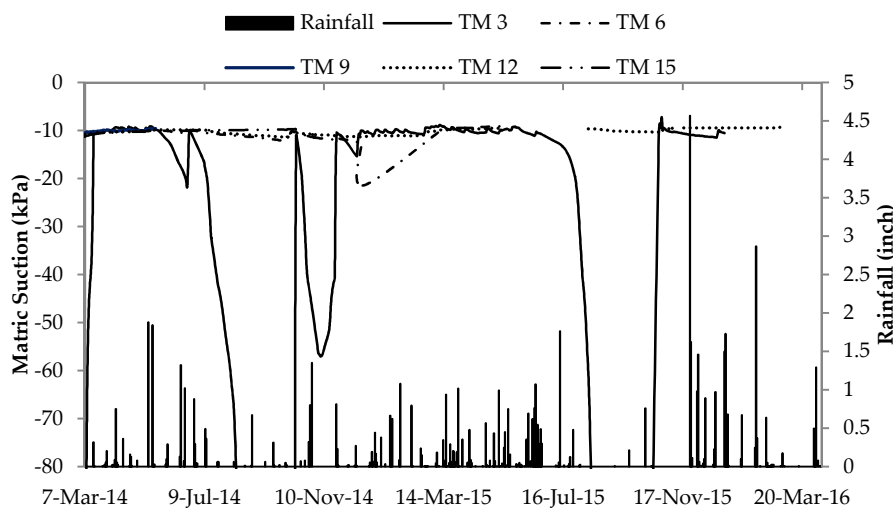


Figure 13. Matric suction at SH 342 site from 2014–16.

Finally, the time/day of the year was evaluated for assessing the effect of seasonal variation in pavement deformation. Past literature has shown that seasonal variation is one of the major causes of volumetric variation in pavement subgrade [12,13,19]. The preceding section about change in resistivity with season authenticates that deformation is dependent upon season/time of the year. The first effort was to enumerate the pavement deformation based on the monitored data.

As mentioned above, the edge being more susceptible to moisture intrusion, only the deformations along the edge were considered for analysis. The field deformations during 2014–16 were plotted as seen in Figure 14a. The plot shows an overall tendency of seasonal variation of deformation with response to rainfall. The seasonal trend, following numerous trials, was found to follow the first-degree Fourier series. The following equation by Reference [35] was solved to estimate the variables.

$$f(t) = a_0 + \sum_{n=1}^{\infty} \left(a_n \cos \frac{2n\pi x}{T} + b_n \sin \frac{2n\pi x}{T} \right)$$

The result of the series followed the form:

$$f(x) = a_0 + a_1 \times \cos(x \times w) + b_1 \times \sin(x \times w)$$

where, a_0 represents the average value of the dataset, a_1 and b_1 are real numbers independent of the variable x , which accounts for the amplitude of the dataset, and w is the frequency (day^{-1}). After numerous trials, a seasonal deformation model was developed as follows:

$$D = 33.56 - 7.751 \times \cos(x \times 0.01854) - 10.4 \times \sin(x \times 0.01854)$$

The model was developed using monitoring data from 2014–15, while the field data from 2015–16 was used to validate the developed model. Figure 14b shows the comparison between actual field data and model predicted values for 2015–16. The model could not predict the significant drop after the summer period, as shown in the figure. However, the typical seasonal change was perfectly depicted by the developed seasonal variation model. This finding points to the necessity of including short-term temporal change in moisture content to obtain better results. The difference in predicted and actual field deformation values suggests that the model should include the effect of rainfall as well.

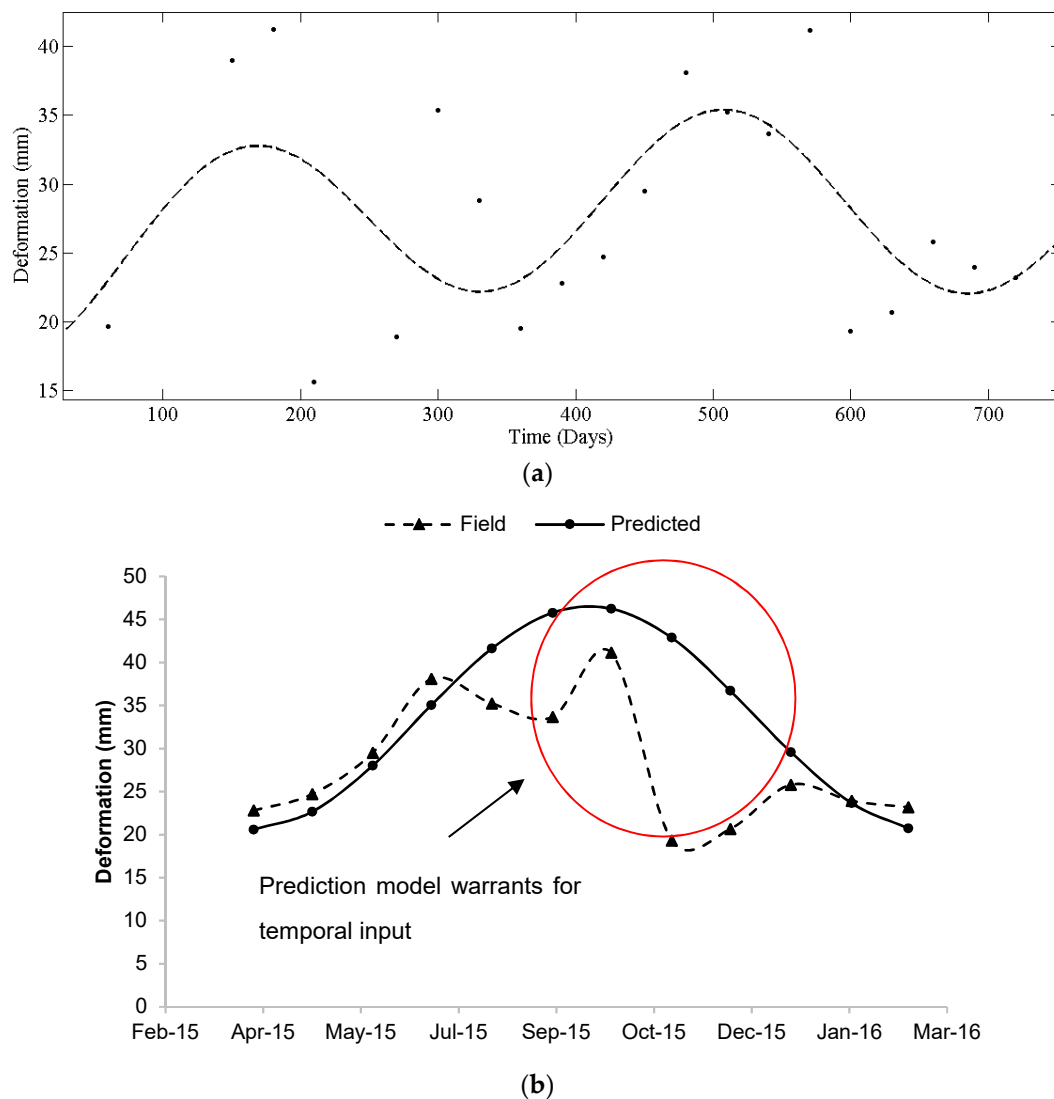


Figure 14. (a) Variation of the edge deformation in 2014–16 period (b) Predicted and field deformation in 2015–16 period.

4.2. Modification of the Model

As discussed above, an attempt was made to improve the prediction model by adding the effect of rainfall. The edge deformation values of 2014–16 (Appendix A) were used to develop the model, while the field data from 2016–17 were used to validate the developed equation. The previous model was modified slightly with the use of new dataset. The frequency (w) changed to 0.01858 and the average value of the dataset (a_0) became 30.56. Consequently, the modified deformation model took the form as follows:

$$D = 30.56 - 7.751 \times \cos(x \times 0.01858) - 10.4 \times \sin(x \times 0.01858)$$

The modified model was validated using the edge deformation of 2016–17. Figure 15 shows the actual field deformations versus the model estimated deformation values. It can be pointed out that there is certain discrepancy in the model and field values for some months. This discrepancy was regarded to have a relation with the precipitation events. Hence, a rainfall factor was estimated by plotting the difference between model and field values on Y-axis and rainfall on X-axis.

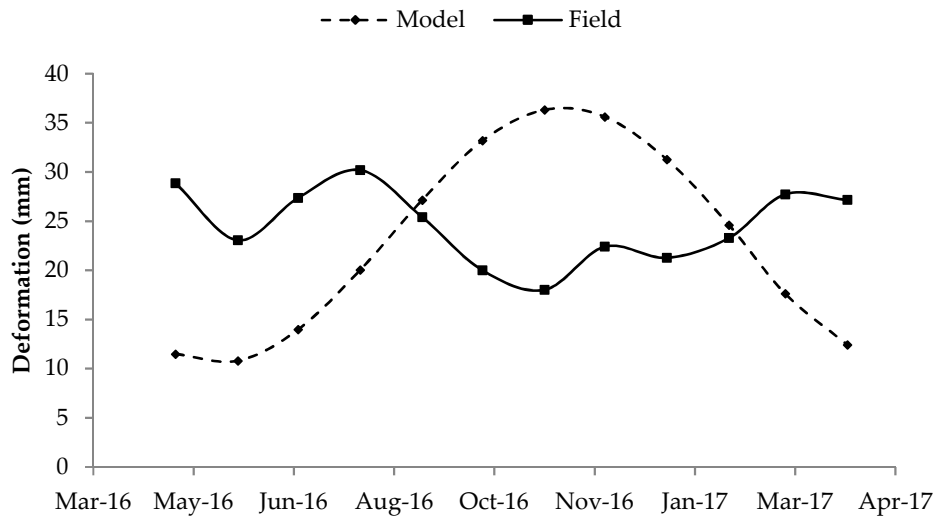


Figure 15. Comparison of model and field results with seasonal effects.

The scatter plot (Figure 16) provided an initial impression of the relation. Starting with linear relation, exponential, power and quadratic relations were tried to estimate the correct rainfall factor. Since none of the trends generated any interpretable result, the log-function transformation was applied initially on both the X and Y axes. This resulted in a limited linear trend in the scatter plot. With a view to improving the accuracy, logarithmic of both squared difference and squared rainfall data were plotted on Y and X axes, respectively. Two different linear trends were detected, with one trend conforming to values when the deformation factor is more than 1, and the other trend being applicable for deformation factors less than 1. Both the equations exhibited coefficient of determination (R^2) more than 0.85. The linear trend equations for both the above-mentioned cases are as follows:

$$y(\text{deformation factor}) = 0.3169 \times (\text{rainfall factor}) + 1.4849$$

$$y(\text{deformation factor}) = 0.7464 \times (\text{rainfall factor}) - 2.221$$

where, y = logarithm of squared difference between the actual and predicted value and x = logarithmic of squared rainfall.

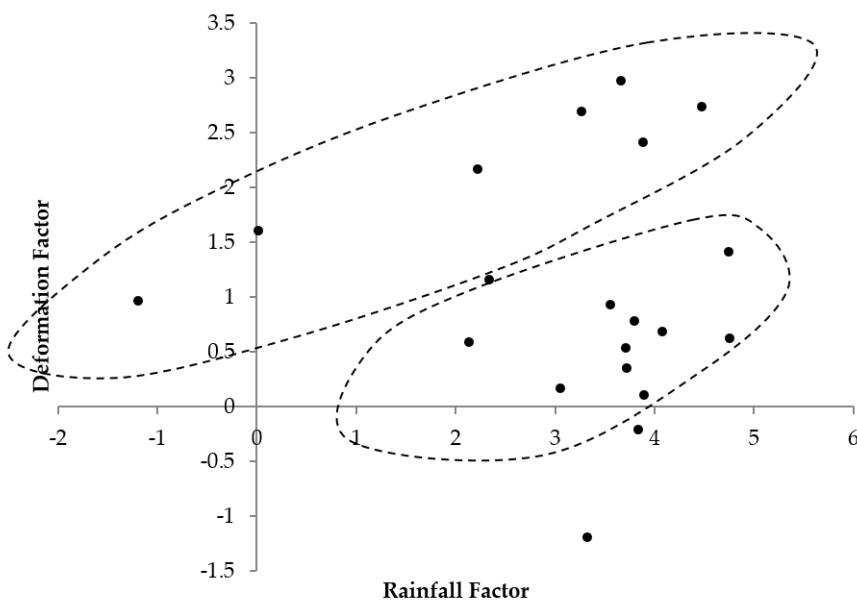


Figure 16. Rainfall factor for model modification.

For instance, the model predicted and actual field deformations in June 2016 were 10.8038 mm and 23.058 mm, respectively. Since the deformation factor was more than 1, the first equation was used. The rainfall in June 2016 (66.8 mm) was squared and the logarithmic value of the squared rainfall was put as 'x' in the equation. The deformation factor 'y' was calculated to be 2.64. Then, the difference in deformation was back-calculated to be 19.92 mm. After adding this factor to 10.80 mm, the final predicted deformation was estimated to be 30.72 mm, which is about 7 mm more than the actual deformation value. Similarly, modified predicted deformation values were also estimated for the remaining months using the same method. A validation plot was again made with final deformation model values and actual field deformations as shown in Figure 17.

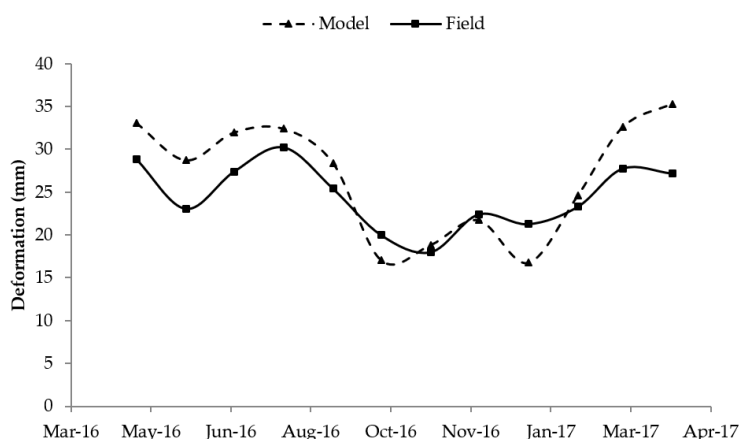


Figure 17. Comparison of model and field results on modified model.

4.3. Statistical Validation of the Deformation Model

It can be stated that the improved model could capture the influence of rainfall effectively. Statistical analysis was performed to further strengthen the model. Hypothesis testing was performed using an independent two-sample t-test to check if a significant difference in actual and predicted mean values existed. A 90% confidence level was assumed for the test. The basic hypothesis of the t-test can be defined as follows:

$$H_0 : m_1 - m_2 = 0$$

$$H_a : m_1 - m_2 \neq 0$$

where,

m_1 = mean of the actual field deformation

m_2 = mean of the model predicted deformation

The test summary presented in Table 1 shows a p-value of 0.332, which is greater than 0.1 (as 90% confidence level was used). Furthermore, the t-value was estimated to be less than the critical value of the two-tailed test. Based on these results, it can be stated that the null hypothesis cannot be rejected. This implies that no significant difference exists between the actual and predicted mean values. Hence, the developed model can be considered successful in capturing the effect of rainfall in the edge deformation.

Table 1. Summary of two-tailed t-test.

| | Mean | Std. Dev. | SE Mean | t-Value | Value |
|-----------|-------|-----------|---------|---------|-------|
| Actual | 24.56 | 3.79 | 1.1 | | |
| Predicted | 26.79 | 6.73 | 1.9 | -1.0 | 0.332 |

4.4. Limitations of the Deformation Model

The model was developed using homogenous soil layers. Additionally, the effect of evaporation on deformation was not analyzed. The incorporation of heterogeneous stratigraphy and the effect of evaporation will further improve the model.

The average deformation values to develop the equation were taken from a specific site. Shrinkage-swelling tests need to be conducted to get approximate average deformation values (X) of other sites as well. This value will replace the first term in the developed model as follows:

$$D = X - 7.751 \times \cos(x \times 0.01858) - 10.4 \times \sin(x \times 0.01858) + \text{Rainfall Factor}$$

where, X is the average deformation value of the site. The sine and cosine part of the equation takes care of the variation of amplitude during swelling and shrinkage of expansive clay. In addition, rainfall factor from the chart will pick the appropriate adjustment value for rainfall events.

4.5. Discussion on the Resilient Modulus

The paper did not include the discussion on resilient modulus change over time due to moisture variation. Previous researchers [36,37] have discussed the wetting-drying cycle and its effect on the resilient modulus (M_R) of soil. The authors conducted the tests in controlled environment in the laboratory with specific boundary conditions (i.e., specific moisture change). However, the current study discusses the ultimate effect of resilient modulus change which is deformation or distress of pavement subgrade. The effect of cyclic wetting and drying is captured in this study by the real-time deformation value collected over the year in the field. In addition, the moisture change is also attributed by the rainfall in real life. As such, the study already captured the effect of change of resilient modulus variation due to moisture variation by recording the deformation over several years.

5. Conclusions and Discussions

The study is related to longitudinal cracks developed as pavement distresses in flexible pavement constructed on expansive subgrade in North Texas. The paper also discusses the influence of moisture on crack development, the intrusion of moisture from edge of pavement, and effect of seasonal variation on recurring crack development. The study statistically and theoretically investigates the associated factors related to pavement deformation. Cracks initiate at the pavement edge since the highest tensile stress develops close to the pavement shoulder, due to which only the edge deformation was considered for developing the model. Temperature, suction, seasonal variation and rainfall were assessed for the deformation model. The preliminary model suggested seasonal variation and rainfall distribution be the governing factors for predicting deformation. The developed model was modified and statistically tested, which showed that the prediction model was in good agreement with the actual field deformations. The following discussions can be inferred based on the main findings in the study:

- Previous studies focused on deformation behavior of expansive subgrade based on laboratory testing and numerical model; this study attempts to develop deformation model based on real-time deformation data collected over three consecutive years.
- As rainfall and change of moisture content are correlated, only rainfall amount was included in the model to avoid multicollinearity. Temperature and suction were also eliminated from the model development as a significant correlation was not attained.
- The influence of trees was discussed in a qualitative manner, and it was excluded from model development.
- Moisture variation data from field instrumentation and resistivity imaging indicated that the edge of the pavement is more vulnerable; as such, the edge deformation model was considered.
- Both seasonal variation and temporal variation due to rainfall were included for the deformation model.

- The initial model can capture the seasonal trend but modification is required to include the rainfall effect in the deformation model.
- Rainfall factor was determined to be included in the final deformation model, which satisfied the validation statistically.
- The model was limited to the assumption of single soil layer/homogeneous stratigraphy. The inclusion of different soil layer and evaporation consideration will further improve the model.

Author Contributions: Conceptualization, A.A. and M.S.H., B.T.; methodology, A.A.; software, A.A.; validation, A.A.; formal analysis, A.A. and M.S.H.; investigation, A.A., M.S.H., B.T., and P.P.; resources, M.S.H.; writing-draft preparation, A.A. and P.P.; supervision, M.S.H.; project administration, M.S.H.; writing- final manuscript preparation, A.S., P.P. All authors read and edited the paper before submission.

Funding: This research was funded by the Texas Department of Transportation (TxDOT), who are gratefully acknowledged here.

Acknowledgments: The authors express their sincere appreciation to Boon Thian, District Pavement Engineer of TxDOT Dallas office for his careful guidance, helpful suggestions and constructive discussions throughout the project.

Conflicts of Interest: The authors declare no conflict of interest.

Appendix A

Dataset for Model Development.

| | Day | Rain | Deformation |
|--------------|-----|------|-------------|
| 14 March | 0 | 1.23 | 0 |
| 14 May | 60 | 3.49 | 0.7746 |
| 14 August | 150 | 2.82 | 1.5354 |
| 14 September | 180 | 0.46 | 1.623 |
| 14 October | 210 | 2.68 | 0.6156 |
| 14 December | 270 | 1.69 | 0.7446 |
| 15 Jane | 300 | 3.26 | 1.3932 |
| 15 February | 330 | 1.33 | 1.1352 |
| 15 March | 360 | 2.35 | 0.768 |
| 15 April | 390 | 4.3 | 0.8976 |
| 15 May | 420 | 9.44 | 0.9726 |
| 15 June | 450 | 2.87 | 1.1622 |
| 15 July | 480 | 0.01 | 1.5 |
| 15 August | 510 | 0.04 | 1.3878 |
| 15 September | 540 | 0.51 | 1.3254 |
| 15 October | 570 | 9.29 | 1.62 |
| 15 November | 600 | 6.84 | 0.7608 |
| 15 December | 630 | 3.44 | 0.8136 |
| 16 Jane | 660 | 0.58 | 1.0158 |
| 16 February | 690 | 1.81 | 0.942 |
| 16 March | 720 | 3.13 | 0.9132 |

References

1. Djellali, A.; Ounis, A.; Saghafi, B. Behavior of flexible pavements on expansive soils. *Int. J. Transp. Eng.* **2013**, *1*, 1–16.
2. Steinberg, M.L. *Further Monitoring of Twelve Geomembrane Sites in Texas*; Texas State Department of Highways & Public Transp: Austin, TX, USA, 1990.
3. Nelson, J.; Miller, D.J. *Expansive Soils: Problems and Practice in Foundation and Pavement Engineering*; John Wiley & Sons: Hoboken, NJ, USA, 1997.

4. Jones, L.D.; Jefferson, I. Expansive soils. In *ICE Manual of Geotechnical Engineering*; ICE Publishing: London, UK, 2012; pp. 413–441.
5. Das, B.M. *Advanced Soil Mechanics*; Crc Press: Boca Raton, FL, USA, 2013; ISBN 978-1-4822-3483-1.
6. Khan, M.S.; Hossain, S.; Ahmed, A.; Faysal, M. Investigation of a shallow slope failure on expansive clay in Texas. *Eng. Geol.* **2017**, *219*, 118–129. [[CrossRef](#)]
7. Chabrilat, S.; Goetz, A.F.; Krosley, L.; Olsen, H.W. Use of hyperspectral images in the identification and mapping of expansive clay soils and the role of spatial resolution. *Remote Sens. Environ.* **2002**, *82*, 431–445. [[CrossRef](#)]
8. Punthuthaecha, K.; Puppala, A.J.; Vanapalli, S.K.; Inyang, H. Volume change behaviors of expansive soils stabilized with recycled ashes and fibers. *J. Mater. Civ. Eng.* **2006**, *18*, 295–306. [[CrossRef](#)]
9. Manosuthikij, T.; Chittoori, B.C. Swell and shrinkage characterizations of unsaturated expansive clays from Texas. *Eng. Geol.* **2013**, *164*, 187–194.
10. Sebesta, S. *Investigation of Maintenance Base Repairs over Expansive Soils: Year 1 Report*; Texas Transportation Institute, Texas A & M University System: Austin, TX, USA, 2002.
11. Hedayati, M. Rainfall induced distress in low volume pavements. Ph.D. Thesis, The University of Texas at Arlington, Arlington, TX, USA, 2014.
12. Ahmed, A.; Hossain, M.S.; Khan, M.S.; Greenwood, K.; Shishani, A. Moisture Variation in Expansive Subgrade Through Field Instrumentation and Geophysical Testing. In Proceedings of the International Congress and Exhibition “Sustainable Civil Infrastructures: Innovative Infrastructure Geotechnology”, Sharm El Sheikh, Egypt, 15–19 July 2017; pp. 45–58.
13. Sapkota, A.; Ahmed, A.; Pandey, P.; Hossain, M.; Lozano, N. Stabilization of Rainfall-Induced Slope Failure and Pavement Distresses Using Recycled Plastic Pins and Modified Moisture Barrier. In Proceedings of the Eighth International Conference on Case Histories in Geotechnical Engineering (Geo-Congress 2019), Philadelphia, PA, USA, March 24–27 2019.
14. Hashem, M.D.; Abu-Baker, A.M.; Hashem, M.D. Numerical Modeling of Flexible Pavement Constructed On Expansive Soils. *Eur Int J Sci Tech.* **2013**, *2*, 19–34.
15. Inclinometer: Casing and Portable Measurement Systems. DGSi. 2018. Available online: <https://durhamgeo.com/inclinometers/> (accessed on 17 October 2019).
16. Bae, A.; Stoffels, S.M.; Antle, C.E.; Lee, S.W. Observed evidence of subgrade moisture influence on pavement longitudinal profile. *Can. J. Civ. Eng.* **2008**, *35*, 1050–1063. [[CrossRef](#)]
17. Manzur, S.R.; Hossain, M.S.; Kemler, V.; Khan, M.S. Monitoring extent of moisture variations due to leachate recirculation in an ELR/bioreactor landfill using resistivity imaging. *Waste Manag.* **2016**, *55*, 38–48. [[CrossRef](#)] [[PubMed](#)]
18. Advanced Geosciences, Inc. *Instruction Manual for EarthImager 2D, Version 2.1. 7, Resistivity and IP Inversion Software*; Advanced Geosciences, Inc.: Saint Antonio, TX, USA, 2004.
19. Hossain, S.; Ahmed, A.; Khan, M.S.; Aramoon, A.; Thian, B. Expansive subgrade behavior on a state highway in North Texas. In Proceedings of the Geotechnical and Structural Engineering Congress 2016 Structural Engineering Institute, Phoenix, AZ, USA, 14–17 February 2016.
20. Hsu, S.-C.; Nelson, P.P. Characterization of eagle ford shale. *Eng. Geol.* **2002**, *67*, 169–183. [[CrossRef](#)]
21. Abrams, T.G.; Wright, S.G. *A Survey of Earth Slope Failures and Remedial Measures in Texas*; Texas State Department of Highways & Public Transp: Austin, TX, USA, 1972.
22. Li, M.; Fang, C.; Kawasaki, S.; Achal, V. Fly ash incorporated with biocement to improve strength of expansive soil. *Sci. Rep.* **2018**, *8*, 2565. [[CrossRef](#)] [[PubMed](#)]
23. Goodarzi, A.R.; Akbari, H.R.; Salimi, M. Enhanced stabilization of highly expansive clays by mixing cement and silica fume. *Appl. Clay Sci.* **2016**, *132*, 675–684. [[CrossRef](#)]
24. Pandey, P.; Ahmed, A.; Sapkota, A.; Hossain, M.S.; Thian, B. Performance Evaluation of Pavement Subgrade by In Situ Moisture and Matric Suction Measurements. In Proceedings of the Eighth International Conference on Case Histories in Geotechnical Engineering (Geo-Congress 2019) American Society of Civil Engineers, Philadelphia, PA, USA, 24–27 March 2019.
25. Ward, W.H. Soil Movements and Weather. In Proceedings of the Third International Conference On Soil Mechanics And Foundation Engineering, Zurich, Switzerland, 16–27 August 1953; Volume 2, pp. 477–481.

26. Manosuthikij, T. Studies on volume change movements in high PI clays for better design of low volume pavements. Ph.D. Thesis, The University of Texas at Arlington, Arlington, TX, USA, 2008.
27. Manosuthikij, T.; Nazarian, S.; Hoyos, L.R.; Chittoori, B. In situ matric suction and moisture content measurements in expansive clay during seasonal fluctuations. *Geotech. Test. J.* **2011**, *35*, 74–82.
28. Wagner, J.-F. Mechanical properties of clays and clay minerals. In *Developments in Clay Science*; Elsevier: London, UK, 2013; Volume 5, pp. 347–381.
29. Luo, R.; Prozzi, J.A. Development of longitudinal cracks on pavement over shrinking expansive subgrade. *Road Mater. Pavement Des.* **2010**, *11*, 807–832. [[CrossRef](#)]
30. Kutner, M.H.; Nachtsheim, C.J.; Neter, J.; Li, W. *Applied Linear Statistical Models*; McGraw-Hill Irwin Boston: Boston, MA, USA, 2005; Volume 5.
31. WP4C Dew Point PotentiaMeter. 2017. Available online: [http://daskumars.com/ProductDetail.aspx?ProductName=WP4%20-%20Water%20Potential%20Meter%20\(Dew%20Point%20Potentiometer\)](http://daskumars.com/ProductDetail.aspx?ProductName=WP4%20-%20Water%20Potential%20Meter%20(Dew%20Point%20Potentiometer)) (accessed on 17 October 2019).
32. Fredlund, D.G.; Rahardjo, H.; Rahardjo, H. *Soil Mechanics for Unsaturated Soils*; John Wiley & Sons: Hoboken, NJ, USA, 1993.
33. Fityus, S.G. A soil moisture-based method of estimating γ_s . In *Proceedings 8th Australia New Zealand Conference on Geomechanics: Consolidating Knowledge*; Australian Geomechanics Society: Sydney, Australia, 1999; p. 809.
34. Kodikara, J.; Rajeev, P.; Chan, D.; Gallage, C. Soil moisture monitoring at the field scale using neutron probe. *Can. Geotech. J.* **2013**, *51*, 332–345. [[CrossRef](#)]
35. Sastry, S.S. *Introductory Methods of Numerical Analysis*; PHI Learning Pvt. Ltd.: New Delhi, India, 2012.
36. Ng, C.W.W.; Zhou, C. Cyclic behaviour of an unsaturated silt at various suctions and temperatures. *Géotechnique* **2014**, *64*, 709–720. [[CrossRef](#)]
37. Najji, K. Resilient modulus-moisture content relationships for pavement engineering applications. *Int. J. Pavement Eng.* **2018**, *19*, 651–660. [[CrossRef](#)]



© 2019 by the authors. Licensee MDPI, Basel, Switzerland. This article is an open access article distributed under the terms and conditions of the Creative Commons Attribution (CC BY) license (<http://creativecommons.org/licenses/by/4.0/>).